Fermi National Accelerator Laboratory

FERMILAB-Pub-87/179-E
[E-741/CDF]

CDF Central Muon Detector*

G. Ascoli, L.E. Holloway, I. Karliner, U.E. Kruse,
R.D. Sard, V.J. Simaitis, D.A. Smith, and T.K. Westhusing

Loomis Laboratory of Physics
The University of Illinois
1110 W. Green Street
Urbana, Illinois 61801

July-August 1987

*Submitted to Nucl. Instrum. Methods A

Operated by Universities Research Association Inc. under contract with the United States Department of Energy

CDF Central Muon Detector

G. Ascoli, L.E. Holloway, I. Karliner, U.E. Kruse,

R.D. Sard, V.J. Simaitis, D.A. Smith, T.K. Westhusing

Loomis Laboratory of Physics*

The University of Illinois

1110 W. Green Street

Urbana, Illinois 61801

Design, construction and performance characteristics of the streamer chambers for the Central Muon Detector at CDF are described. A single hit TDC is used for measurements in the drift (azimuth) direction while charge division is used for measurements along the sense wire (pseudorapidity). The chambers operate in the limited streamer mode with a 50%/50% ratio of argon/ethane bubbled through ethanol. Measurements in a cosmic ray test stand, pion test beam and as part of the CDF detector indicate a rms resolution of 250 microns in the drift direction and a rms resolution of 1.2 millimeters along the sense wire are attainable.

*This work was supported by the U.S. Department of Energy, Contract No. DE-AC02-76ER01195

CDF Central Muon Detector

1. Introduction

In this article we will describe the drift chambers for muon detection in the central rapidity region, $| y | \leq 0.7$, of the CDF detector. These chambers identify muons by their penetration of the 4.9 absorption lengths of the central calorimeter, measure their positions and directions, and provide a level-one trigger for muons which have a transverse momentum greater than a given set value. In section 2 of this paper, we describe the chamber geometry and how the level-one trigger is achieved. In section 3, we describe the method of construction and in section 4, the method of charge division is outlined. Section 5 contains some results obtained with cosmic ray and test beam data.

2. Geometry

The central muon detector is located around the outside of the central hadron calorimeter at a radial distance of 3470 mm from the beam axis. The muon detector is segmented in phi into 12.6° wedges which fit into the top of each central calorimeter wedge. This leaves a gap in the central muon coverage of 2.4° between each wedge. Access to the muon detector is through a 300 $mm \times$ 120 mm opening at each end of the central calorimeter wedge so that each detector is further segmented in phi into three modules of 4.2° each. The three modules are bolted together at each end to form a single unit. This single unit is suspended from the top of the calorimeter wedge at three points which provide for adjustment of the chambers in both θ and ϕ.[1] Figure 1 illustrates the muon chambers in each wedge.

Each of the three modules in a wedge consists of four layers of four rectangular drift

cells. A typical drift cell is shown in figure 2. Overall dimensions of the cell are 63.5 mm wide $\times$ 26.8 mm high $\times$ 2261 mm long. A stainless steel resisitive 50 μm sense wire is located at the center of the cell.

Arrangement of the sense wires within a muon chamber permits a lower bound on the transverse momentum of a particle to be determined. Four sense wires, one from each layer, make up a muon tower (figure 3). Two of the four sense wires, from alternating layers, lie on a radial line which passes through the interaction point. The remaining two wires of the tower lie on a radial line which is offset from the first by 2 mm at the midpoint of the chamber. The ambiguity as to which side of the sense wires (in ϕ) a track passes is resolved by determining which two sense wires were hit first. The angle α between a particle track and the radial line passing through the sense wires can be determined by measuring the difference in arrival times of the drift electrons. A muon tower therefore provides two independent measurements of α.

Figure 4 shows a transverse projection of a track as a particle passes through the central solenoidal magnetic field. From figure 4, one can derive the relationship between α and β, where β is the angle of deflection due to the magnetic field. This relation is given by

$$D\sin(\alpha) = L\sin(\frac{\beta}{2}), \tag{1}$$

where D = 3470 mm is the distance from the interaction point to the bottom of the muon detector and L = 1440 mm is the radius of the solenoidal magnetic field.

The angle β in turn can be related to the transverse momentum of a particle. If B = 1.5 T is the magnitude of the magnetic field and P_t is the transverse momentum of the

particle, then

$$\sin(\frac{\beta}{2}) = \frac{eLB}{2P_t} \tag{2}$$

Equations (1) and (2) when combined give α in terms of P_t

$$\alpha \simeq \sin(\alpha) = \frac{eL^2B}{2DP_t}$$

The relationship between α and the difference in drift times, Δs, for two sense wires in alternating layers is given by

$$\Delta s = \frac{H\alpha}{v}$$

where H = 55.0 mm is the separation of the sense wire layers, and v is the drift velocity of the ionization electrons.

Δs is compared to a preset value in the RABBIT muon level - one trigger card[2]. If Δs is less than this value, a level - one trigger signal is generated.

3. Chamber Construction

The top and bottom of a drift cell consist of 0.79 mm thick aluminum sheets which span the width of the muon chamber. The sheets are held at ground through small brass 90° angle joints which are connected to the sheets and the aluminum chamber end plates with conductive epoxy. The sides of the cell consist of 25.4 mm aluminum I-beams (C-beams for those cells at the side of chamber) which are electrically insulated from the top and bottom sheets with 0.62 mm thick G-10 strips. The I-beams and C-beams are held at -2500 V. In the center of the cell is a 50 μm stainless steel sense wire with a resistance of 0.4 Ω-mm^{-1}. The sense wire enters the cell through the chamber end plate and is electrically insulated from it by a delrin sleeve. A hollow brass pin in the middle of the

sleeve is crimped around the wire to hold it in place. The wire is place under a tension of 110 gm which limits the wire sag to 90 μm. The sense wire is normally held at +3150 V.

Figure 5 shows the electric field as a function of distance from the wire along a horizontal line passing through the center of the cell. The local minimum in the electric field near the wire is sensitive to the cell width and is also sensitive to the width of the top and bottom of the I-beams. The minimum in the field closest to the I-beam is primarily sensitive to the width of the top and bottom of the I-beam. Because our sense wire arrangement requires cell widths ranging from 56.6 mm to 67.8 mm, adjustment of the I-beam width is necessary to insure that the electric field at the wire is the same for all cells. A minimum field strength of 100 $V\text{-}mm^{-1}$ is required to maintain a constant drift velocity in 50%/50% argon-ethane gas with 0.7% ethanol.[3]

Charge division is used to obtain the position of a track along the sense wire. In order to reduce the number of electronics channels and to enable readout of the chambers to occur at one end of the chamber only, each sense wire is connected at the 90° θ end to a sense wire in the same layer which is separated from the first by an intervening drift cell (figure 6). At each 56° θ end of the wire is a 0.1 μF blocking capacitor which in turn is connected to the RABBIT muon ADC-TDC cards.[4] The blocking capacitors for all channels of a chamber reside in a single package which bolts on to the 56° θ end of the chamber. This package also contains the positive HV connector and readout cable connectors. A smaller package bolted on to the 90°θ end contains the negative HV connector and distribution pads for the I-beams in each of the four layers. The electrical connections between the sense wires and the electronics packages are made with flexible cylinders made of conductive epoxy

which fit over the brass pins holding the sense wires and butt up against distribution pads on the electronic packages.

A total of 180 muon chambers or 60 wedges were constructed. An individual chamber is constructed starting with the layer furthest from the beam axis. The two aluminum endplates are mounted on a fixture which holds them precisely 2261 *mm* apart. An aluminum sheet 254 *mm* wide by 2286 *mm* long is glued on to the endplates with epoxy to form the top of the chamber. G-10 strips 112 *mm* wide by 2274 *mm* long are glued on to form the sides of the chamber. The endplates and acompanying sheets are then transferred to a fixture on a granite table which rigidly holds the end plates and sheets in the desired rectangular shape. C-beams are glued in on each side of the chamber and form the outer walls of the drift cells at the sides of the layer. The location of each of the three I-beams in a layer is determined by spacers which place the I-beam the correct distance from the I or C-beam already in place. An automatic gluing machine then lays down a bead of Eastman 910 along the entire length of the chamber. Another device with jaws which hold an I-beam straight along its entire length then presses the I-beam in place with air cylinders. The C and I-beams are internally connected together with jumper wires which connect adjacent beams so that only one negative HV feedthrough is needed for each layer of beams. An aluminum sheet is then glued on top of the I and C-beam to form the top of the cells and complete the layer. Holes have been cut in the interior aluminum sheets to allow gas to pass between layers. Each of the four layers is built up in this manner until the chamber is complete. The chamber is then strung with the sense wires which have 110 *gm* of tension on each.

The tension of each wire is checked by placing a portion of the chamber in a magnetic field and driving the wires with an alternating voltage as in figure 7. A lock-in amplifier is used to monitor the in phase component, V_{in}, and the out of phase component, V_{out}, of the voltage drop across $R_T = 50\ \Omega$ resistance relative to the driving voltage. The lowest resonance frequency of the sense wire is given by

$$\omega_\circ = \frac{2\pi\sqrt{T/\rho}}{2L} \simeq 2\pi \times 58\ Hz,$$

where T = 110 gm is the tension of the wire; $\rho = 1.55 \times 10^{-5}\ gm\text{-}mm^{-1}$ is the linear mass density of the wire; and L = 2261 mm is the length of the wire. It can be shown that if the frequency of the driving voltage, ω, is near that of the resonance frequency, $\omega_\circ$, then V_{in} is given by

$$V_{in} = \frac{R_T V_\circ}{R_T + R_{wire}}\left(1 + \frac{\omega\beta\tau}{(\omega - \omega_\circ^2/\omega)^2\tau^2 + 1)}\right)$$

and V_{out} is given by

$$V_{out} = \frac{R_T V_\circ \omega\beta\tau^2}{R_T + R_{wire}} \frac{(\omega - \omega_\circ^2/\omega)}{(\omega - \omega_\circ^2/\omega)^2\tau^2 + 1}$$

where $V_\circ$ is the magnitude of the driving voltage; τ is the damping time for the wire; $R_{wire} = 904\ \Omega$ is the wire resistance and

$$\omega_\beta = \frac{B^2 l^2}{M R_{wire}} \tag{3}$$

In equation (3), B is the magnetic field; l is the length of wire in the field; and M is the mass of the wire. The important point to notice is that V_{out} vanishes at resonance while V_{in} attains a maximum. The resonant frequency of the wire can therefore be determined by sweeping the frequency of the alternating voltage over a range of values until V_{out} vanishes and V_{in} attains a maximum.

4. Charge Division

The position of a track along the sense wire is found by charge division. If a streamer pulse, with total charge, Q_0, drifts to the wire from a point X mm from the 90°θ end of the chamber on wire 1 (figure 6) then the total charge collected in ADC1 is given by

$$Q_1 = \frac{Q_0}{2}\,(1 + \frac{X}{L}) \tag{4}$$

and the charge reaching ADC2 is

$$Q_2 = \frac{Q_0}{2}\,(1 - \frac{X}{L}) \tag{5}$$

where L is the length of the unpaired wire. The ratio

$$R = \frac{Q_1 - Q_2}{Q_1 + Q_2} = \frac{X}{L}$$

is then linearly dependent on X. Because the input impedances of the charge amplifiers on the RABBIT muon cards are not zero, the absolute value of R does not range from zero to one but attains a maximum value somewhat less than 1. Another important effect on R is due to the exponential decay ($\tau = CR_{wire}$) of the charge accumulated on each of the 0.1 μF blocking capacitors at the ends of the wire pair. This leads to modification of equations (4) and (5) of the form

$$Q_1 = \frac{Q_0}{2}\,(1 + \frac{X}{L}\,e^{-t/\tau})$$

and the charge reaching ADC2 becomes

$$Q_2 = \frac{Q_0}{2}\,(1 - \frac{X}{L}\,e^{-t/\tau})$$

R is then given by

$$R = \frac{X}{L}\, e^{-t/\tau} \tag{6}$$

The time, t, in equation (6) is the time interval measured by the TDC's so that R can be corrected for the charge decay. X is then a function of R of the form

$$X = AR + B$$

where $A = L$ and $B = 0$.

In general there are variations in wire resistance and the location at which the sense wires have been crimped is not known. It is therefore necessary to calibrate the charge division (i.e. derive A and B) for each wire. To accomplish this calibration, Fe^{55} sources have been placed in two of the three I-beams of each layer so that each drift cell has a source 75 mm from each end directed into the cell (figure 6). Each Fe^{55} source (5.9 KeV γ ray source) produces an interaction in the cell at the rate of about 30 Hz. Source runs are taken in which plots are made of the number of events as a function of R for each source. A gaussian plus background curve is fit to each source plot and the mean location in R of each source is determined. Figure 8 shows the location, in R, of the four sources in a muon tower. If R_1 is the mean value in R of the source at a distance of D_1 along the wire and R_2 is the mean value of the source at D_2 along the wire then $A = (D_2 - D_1)/(R_2 - R_1)$ and $B = D_1 - A \times R_1$ are determined for each wire.

5. Chamber Performance

As part of the checkout procedure of the muon chambers, each chamber goes through a cosmic ray test stand. The test stand set up is illustrated in figure 9. The chambers

operate in the limited streamer mode with the sense wires at +3150 V and -2500 V on the beams. The top and bottom chambers are used to reconstruct a cosmic ray track which is then projected into the center chamber undergoing testing. The sense wires are divided into 50 *mm* segments and an efficiency is found for each segment. Figure 10 shows the results for a typical wire. The wire shows a drop in efficiency at the ends of the chamber due to the distortion of the electric field there.

A cosmic ray run was taken with the muon chambers at $\phi = 67.5°$ and $\phi = 82.5°$ in the CDF detector. The muon level - one trigger card was set up to require a coincidence of all four layers in each muon tower. Prior to the cosmic ray run, source runs were taken and A and B were determined for each sense wire. Figure 1 shows the local coordinate system used in the following analysis.

For a cosmic ray track, the projection of the track into the ZY plane was fit using charge division information from four sense wires in a muon tower. Resolution of the chamber along the wire was determined from a plot of the residuals of the fit for all wires in the wedge at $\phi = 67.5°$. Figure 11 shows a plot of the scaled residuals for the fit in the ZY plane. Because the sigma of a residual plot tends to underestimate the resolution, the residual for each wire is multiplied by a layer dependent factor which compensates for this underestimation. The residuals for layers 0 and 3 were multiplied by 1.83 while the residuals for the two middle layers, 1 and 2, were multiplied by 1.20. Figure 11 gives an rms resolution along the wire of 1.2 *mm*.

A similar situation exists for the fit in the drift direction (XY plane). The calibration constants needed for fitting a track in the drift direction are the drift velocity and time

zero, where time zero is the drift time of an event which passes through the sense wires. For technical reasons, time zero could not be determined for this cosmic ray run. The drift velocity, however, can be determined by comparing the difference in time between streamer pulses arriving at the wires which are offset by 2 mm from each other in a muon tower. Refering to figure 3 where T_i is the drift time for wire i, a plot of the quantity

$$\delta = \frac{T_1 - 3T_2 + 3T_3 - T_4}{4}$$

will have a double peak since tracks on different sides of the sense wires have a delta of opposite sign. The two peaks are separated in space by twice the offset of the wires (2 mm) so that the drift velocity is given by 4 mm divided by the difference in time between the two peaks. Figure 12 shows a plot of number of events as a function of δ for a typical tower. Figure 13 shows the scaled residual plots of the fit in the drift direction for all the wires in the wedge. The rms resolution in the drift direction from this plot is 250 μm.

Data was also taken with the muon chambers when the central calorimeter wedges were undergoing calibration in a pion test beam. The central calorimeter was placed on a hydraulic table which allowed the wedge to be moved in both theta and phi. The beam pipe was directly over the pivot point of the table so that beam could be directed into each central calorimeter tower. Figure 14 is a plot of the ADC distribution from the chambers. The single streamers peak at about 90 pC while a double streamer peak is seen at about 160 pC. The valley in the distribution at about 30 pC is taken as the cut off for valid hits in the ADC's.

The pion energies ranged from 15 to 50 GeV so the punch-through probabilities as a function of pion energy could be studied. For each run, the beam was directed into the

center of tower 2 of the central calorimeter wedge. At tower 2, there is the equivalent of 109 *cm* of iron. Figure 15 is a scatter plot of energy deposition in the hadron calorimeter vs energy deposition in the electromagnetic calorimeter for 50 GeV pions which produced at least two hits in the muon chamber. Those particles with total energy deposition less than 3000 ADC counts ($\simeq$ 7 GeV) were assumed to be muons and were removed from the sample of punch-through candidates. The remaining events were analysed for at least two hits in the muon chamber and a ratio of (number of events showing hits in the muon chamber)/(the total number of pion candidates) is found for each energy of beam. Figure 16 is a plot of this ratio as a function of beam energy. Data from Bodek[5] for 110 *cm* of Fe is plotted for comparison. With the beam in calorimeter tower 2, the muon chambers extend about 100 *cm* on either side of the beam in the θ direction. In ϕ however, the chambers only extend 38 *cm* to either side of the beam axis. To insure that no punch-through was lost by exiting through the side of the wedge and not through the muon chamber, a plot was made (figure 17) of number of events versus cell number (in ϕ) from the beam axis for the particle which passed closest to the beam axis in a punch-through event. Each increment in cell number is an additional 63.5 *mm* from the beam axis. Figure 17 indicates that very few punch-through events fail to intersect the muon chambers so that the punch-through probabilities are correctly reflected in figure 16.

Figure 18 is a plot of the number of tracks per event found for tracks in the drift direction (xy view) for 50 GeV data.

6. Conclusion

In summary, the CDF muon chambers give adequate resolution in the drift direction

of $\sigma = 250\ \mu m$ and exceptional resolution along the sense wire of $\sigma = 1.2\ mm$. It is hoped that difficulties with hadronic punch-through can be overcome through the use of a programmable transverse momentum cut.

A full test of this trigger scheme is expected to come in late 1986 when the fully instrumented CDF detector begins to observe proton-antiproton collisions at 1.6 Tev.

Figure Captions

Figure 1. Location of the Central Muon Chambers within the central calorimeter.

Figure 2. Central muon drift cell.

Figure 3. Track traversing a muon tower. Because sense wires in alternating layers are offset by known amounts, the drift velocity can be determined by comparing differences in drift times for alternating layers.

Figure 4. Transverse projection of a charged particle track. Within the inner circle of radius L = 1440 mm is a 1.5 T magnetic field. The outer circle of radius D = 3470 mm represents the bottom sense wire plane of the muon drift chambers.

Figure 5. Electric field as a function of distance from the sense wire. A plot for cylindrical cell geometry is given for comparison.

Figure 6. Three drift cells in a plane. The sense wire length, L, is 2260 mm. The Fe^{55} sources are used for calibration of charge division.

Figure 7. The sense wire tension is tested by driving the sense wire with a voltage of variable frequency and monitoring the in phase and out of phase component of the voltage drop across the 50 Ω resistor. The in phase component achieves a maximum at resonance while the out of phase component is zero.

Figure 8. Location in R of the four Fe^{55} sources for a sense wire pair.

Figure 9. Cosmic ray test stand setup. The top and bottom chambers define a track which is extrapolated into the test chamber. Efficiencies for each sense wire can then be determined. The scintillators provide the trigger.

Figure 10. Efficiency as a function of R for a typical sense wire. The wire becomes inefficient at the ends due to the distorted electric field.

Figure 11. Plot of residuals for tracks using charge division information. The rms resolution along the sense wire is 1.2 mm.

Figure 12. A plot of δ for cosmic rays. The separation of the two peaks in time represents a separation of twice the sense wire offset in space.

Figure 13. Plot of residuals for tracks using drift time information. The rms resolution in the drift direction is 250 μm.

Figure 14. ADC pulse height distribution.

Figure 15. Scatter plot of energy deposition in the hadron calorimeter vs. electromagnetic calorimeter for 50 Gev pions. Muon candidates deposit less than 7 Gev in the calorimetry.

Figure 16. Punch-through probability as a function of pion energy for the CDF calorimeter. Data from Bodek[5] is plotted for comparison.

Figure 17. Distribution, as a function of drift cell number, of punch through particles in the muon chamber. Each drift cell increment represents an additional 63.5 mm from the beam axis.

Figure 18. Number of tracks found per event using drift information for 50 Gev pions.

References

1. CDF NIM paper, section 4.1.1 'An Alignment System for the Central Muon Chambers'

2. CDF NIM paper, section 7.3.2 'CDF Central Muon Trigger Level 1 Electronics'

3. Muzaffer Atac, private communication

4. CDF NIM paper, section 7.3 'Rabbit Front End Electronics'

5. A. Bodek, University of Rochester preprint UR911 (1985); to be published in Proc. Workshop for Muon Identification at the SSC, Madison, Wisconsin (1985).

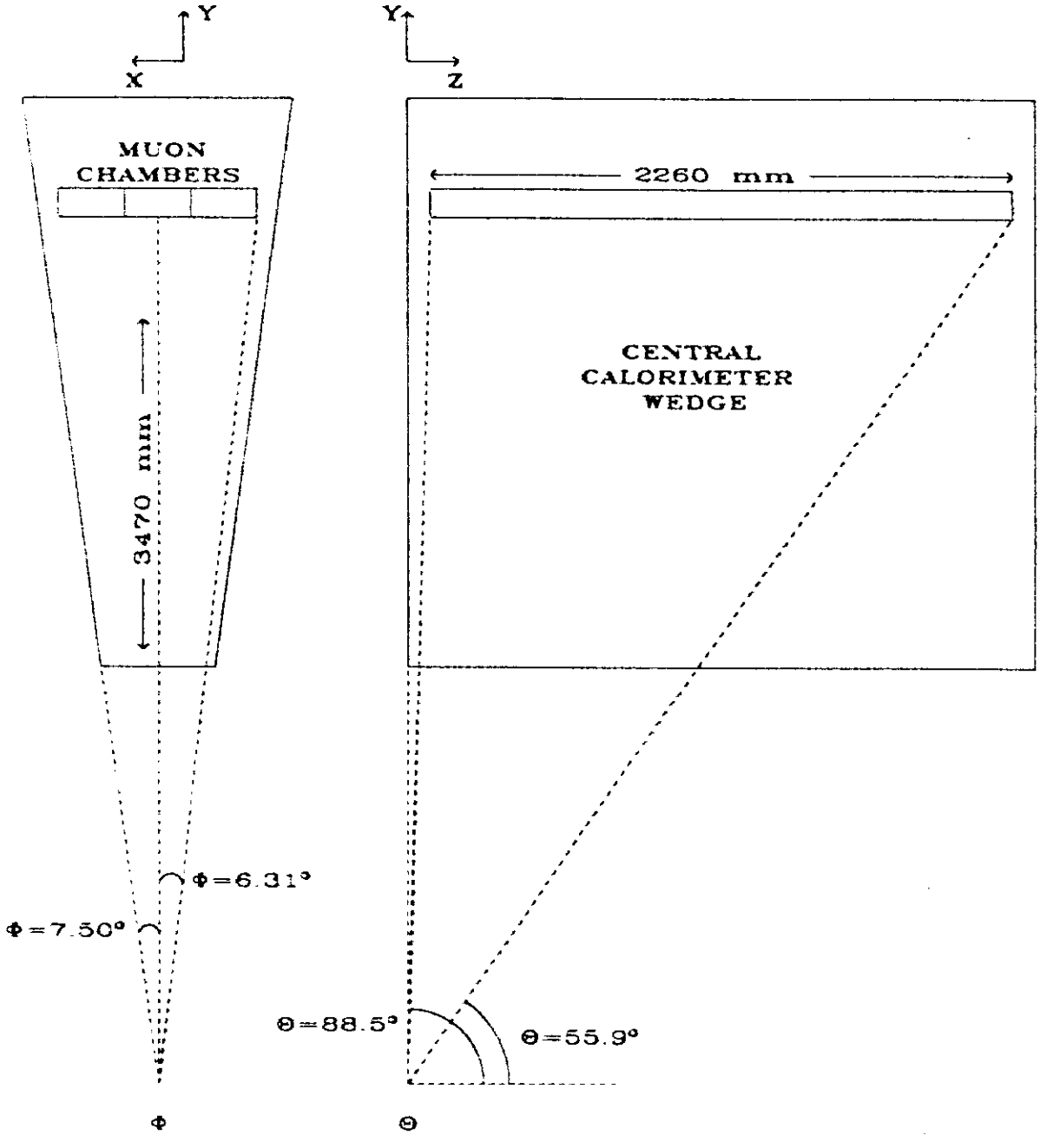
Y
X
Y
Z
MUON
CHAMBERS
2260 mm
CENTRAL
CALORIMETER
WEDGE
3470 mm
Φ=6.31°
Φ=7.50°
Θ=88.5°
Θ=55.9°
Φ
Θ

Fig. 1

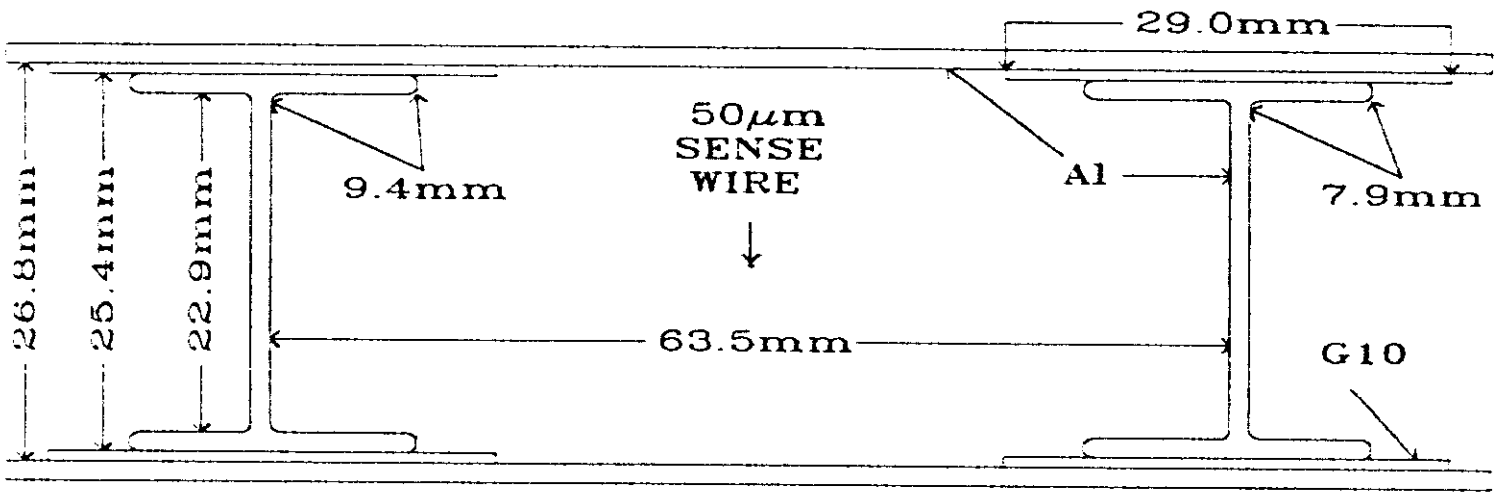
29.0mm
26.8mm
25.4mm
22.9mm
9.4mm
50μm
SENSE
WIRE
Al
7.9mm
63.5mm
G10

Fig. 2

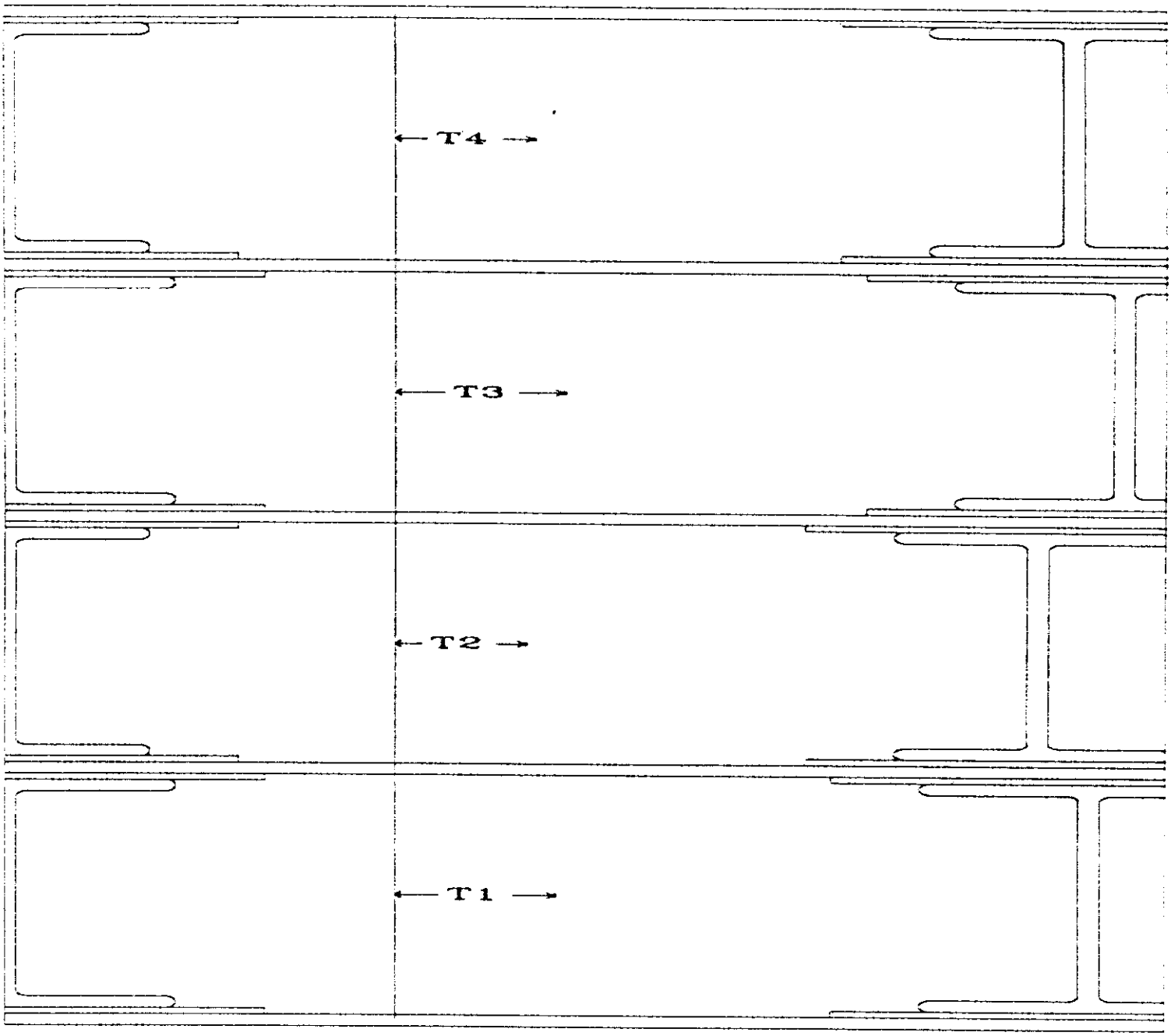

Fig. 3

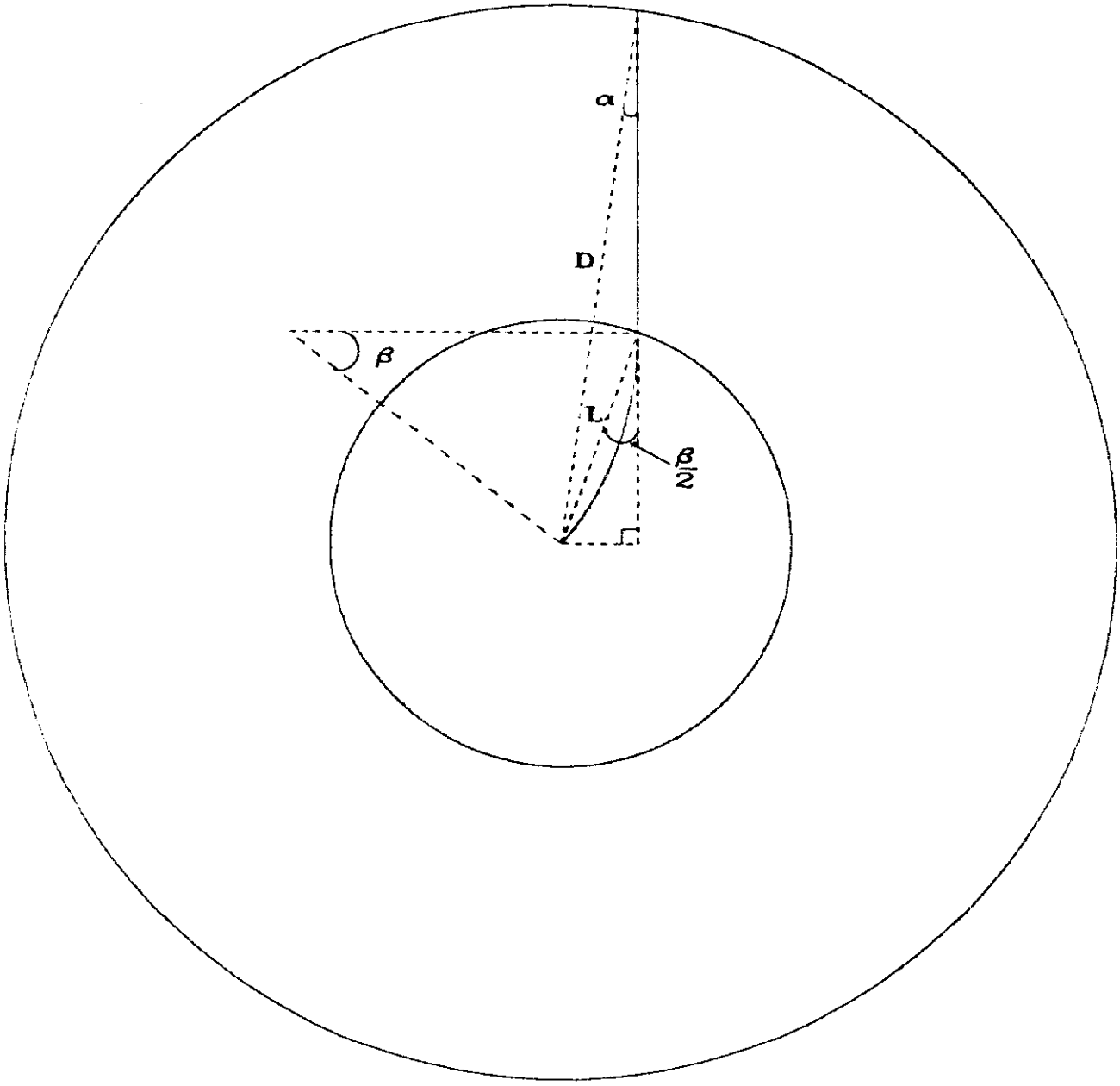

Fig. 4

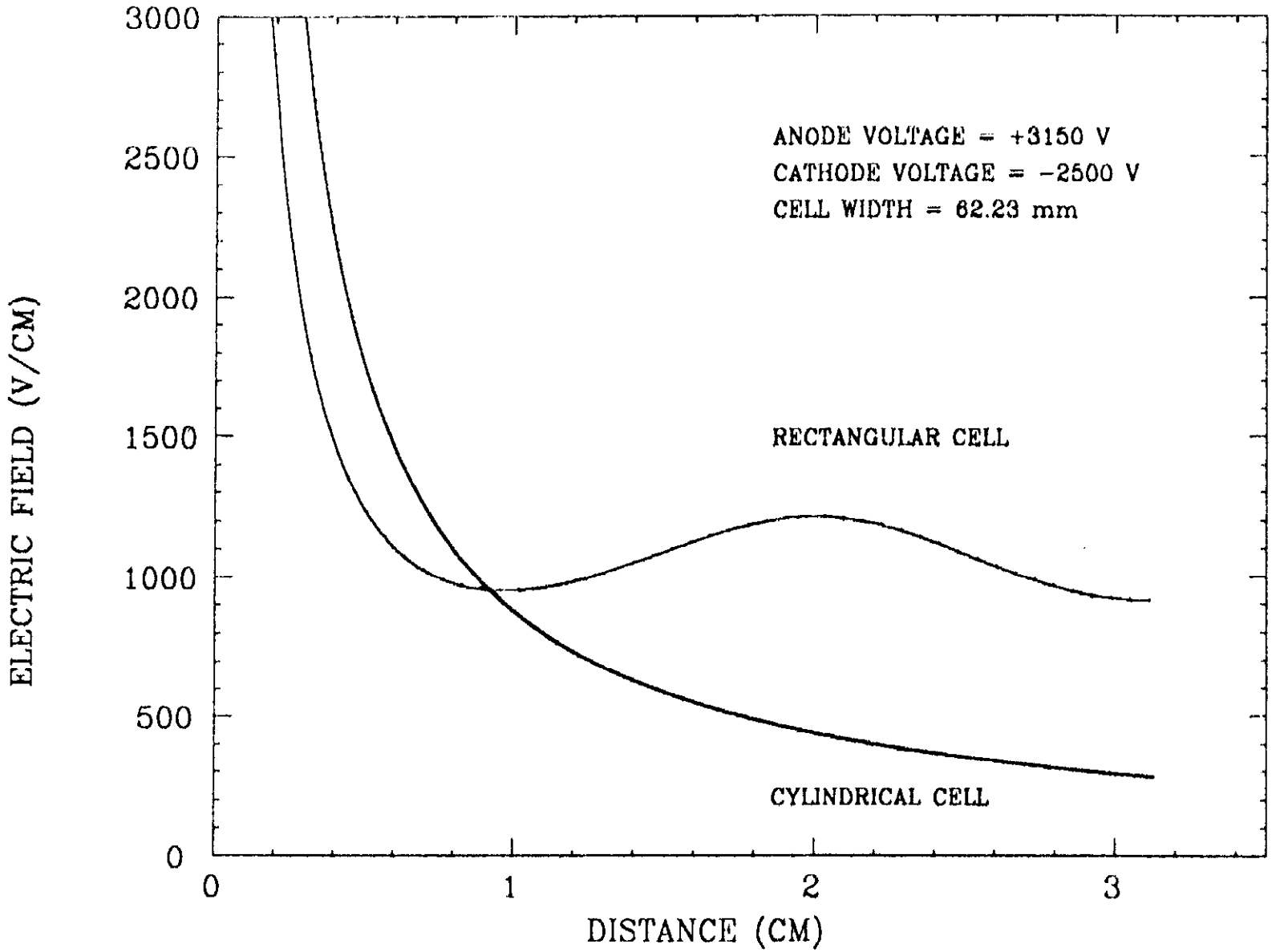
ELECTRIC FIELD (V/CM)
3000
2500
2000
1500
1000
500
0
0
1
2
3
DISTANCE (CM)
ANODE VOLTAGE = +3150 V
CATHODE VOLTAGE = -2500 V
CELL WIDTH = 62.23 mm
RECTANGULAR CELL
CYLINDRICAL CELL

Fig. 5

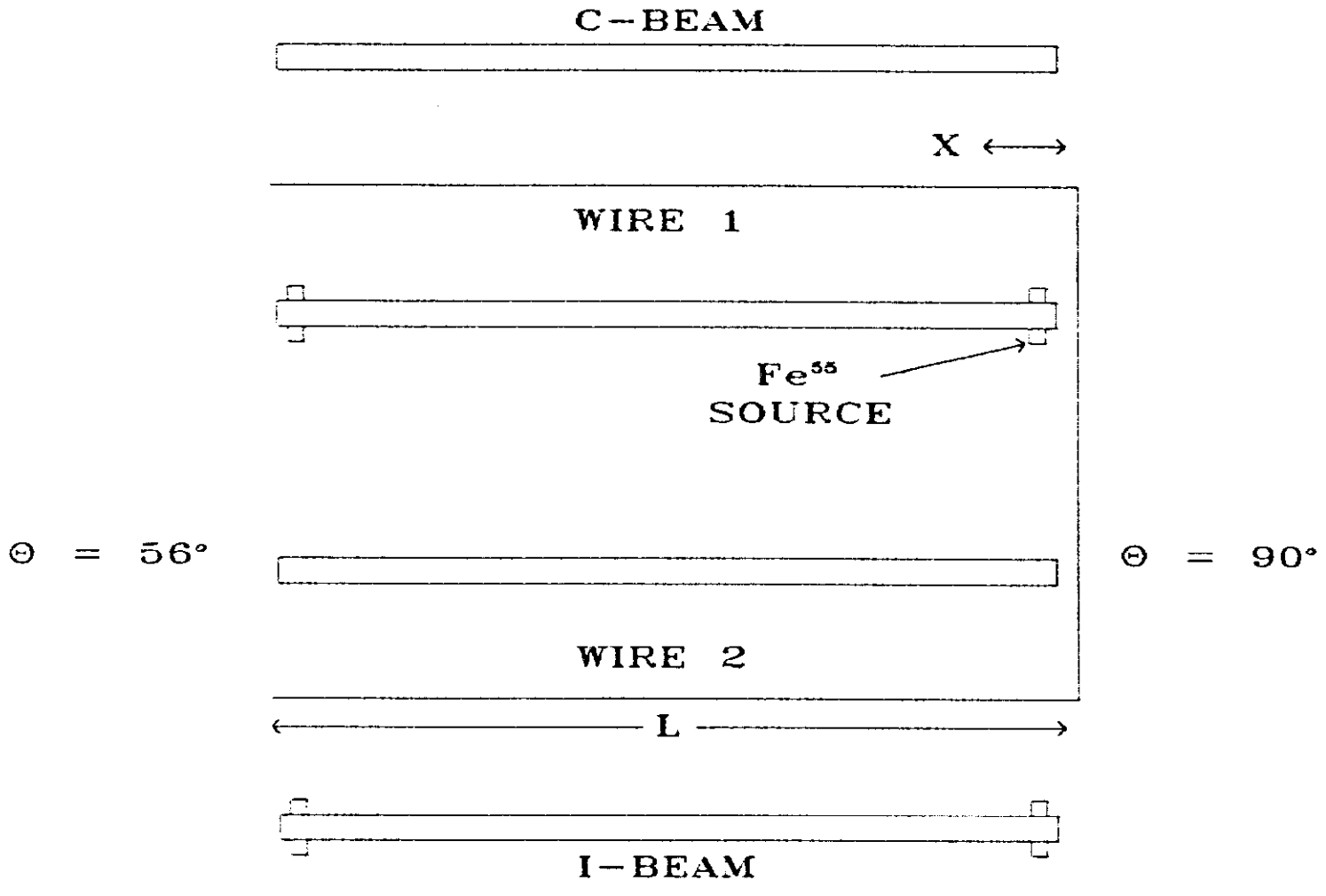

Fig. 6

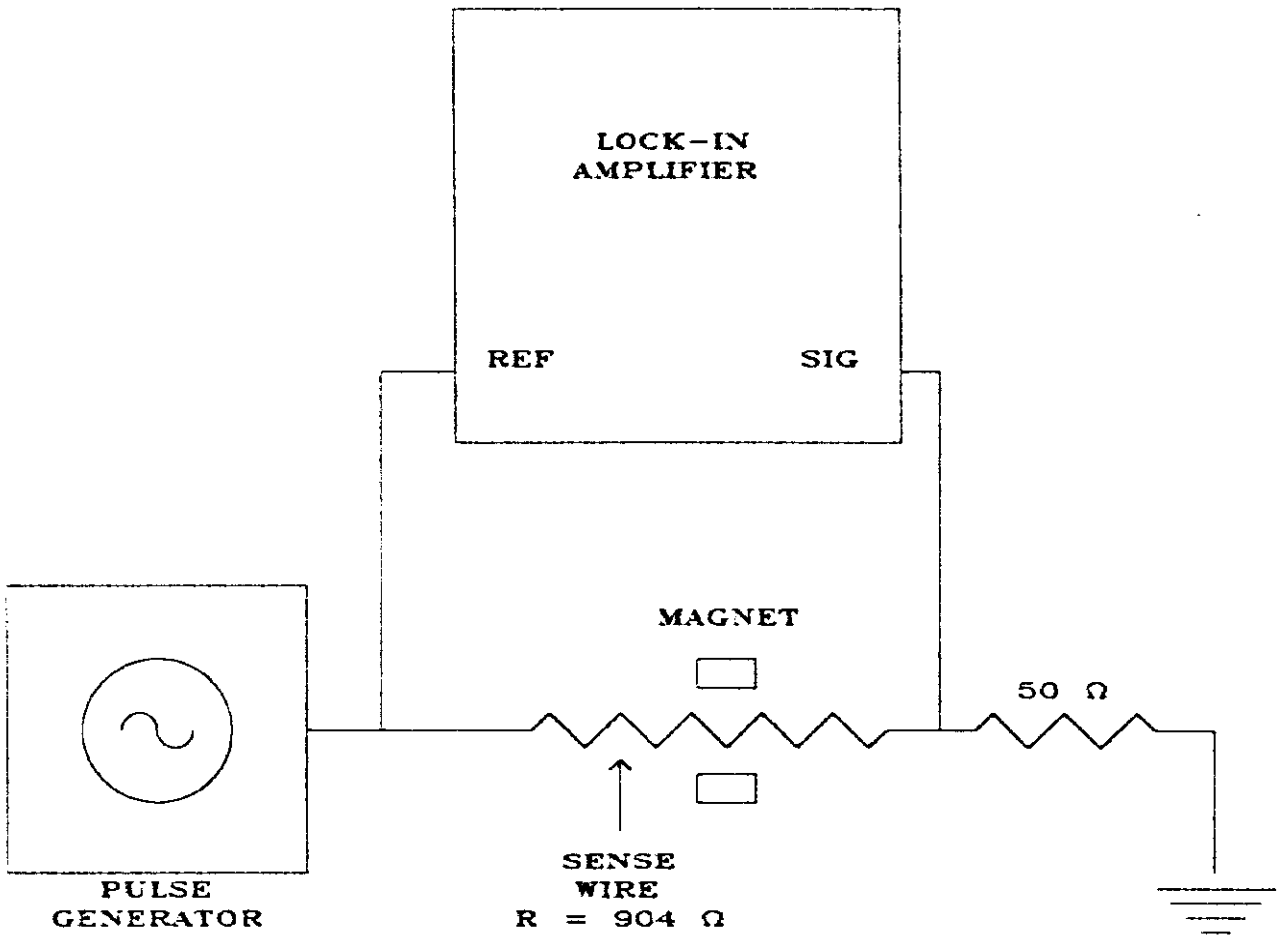
LOCK-IN
AMPLIFIER
REF
SIG
MAGNET
50 Ω
PULSE
GENERATOR
SENSE
WIRE
R = 904 Ω

Fig. 7

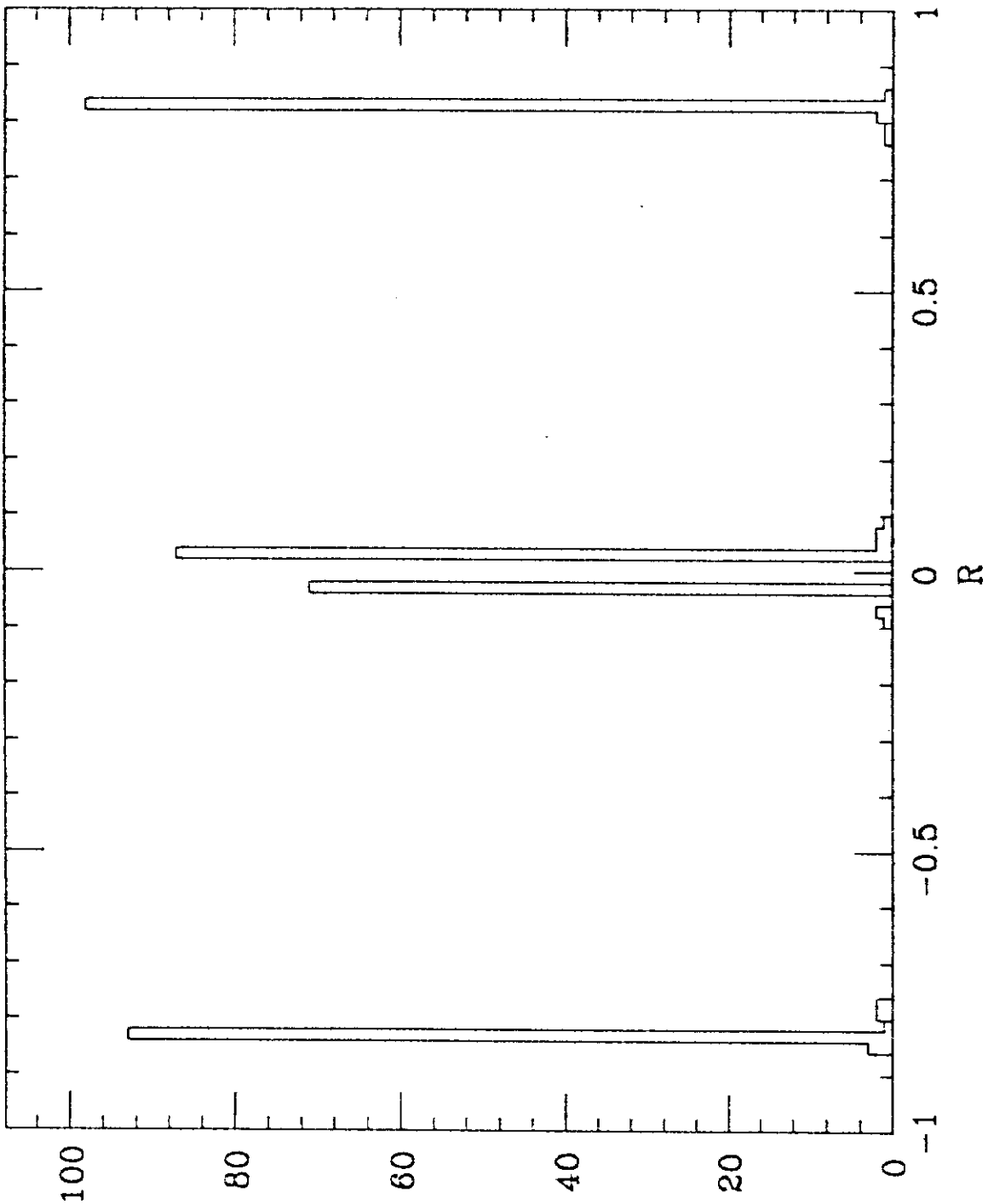

Fig. 8

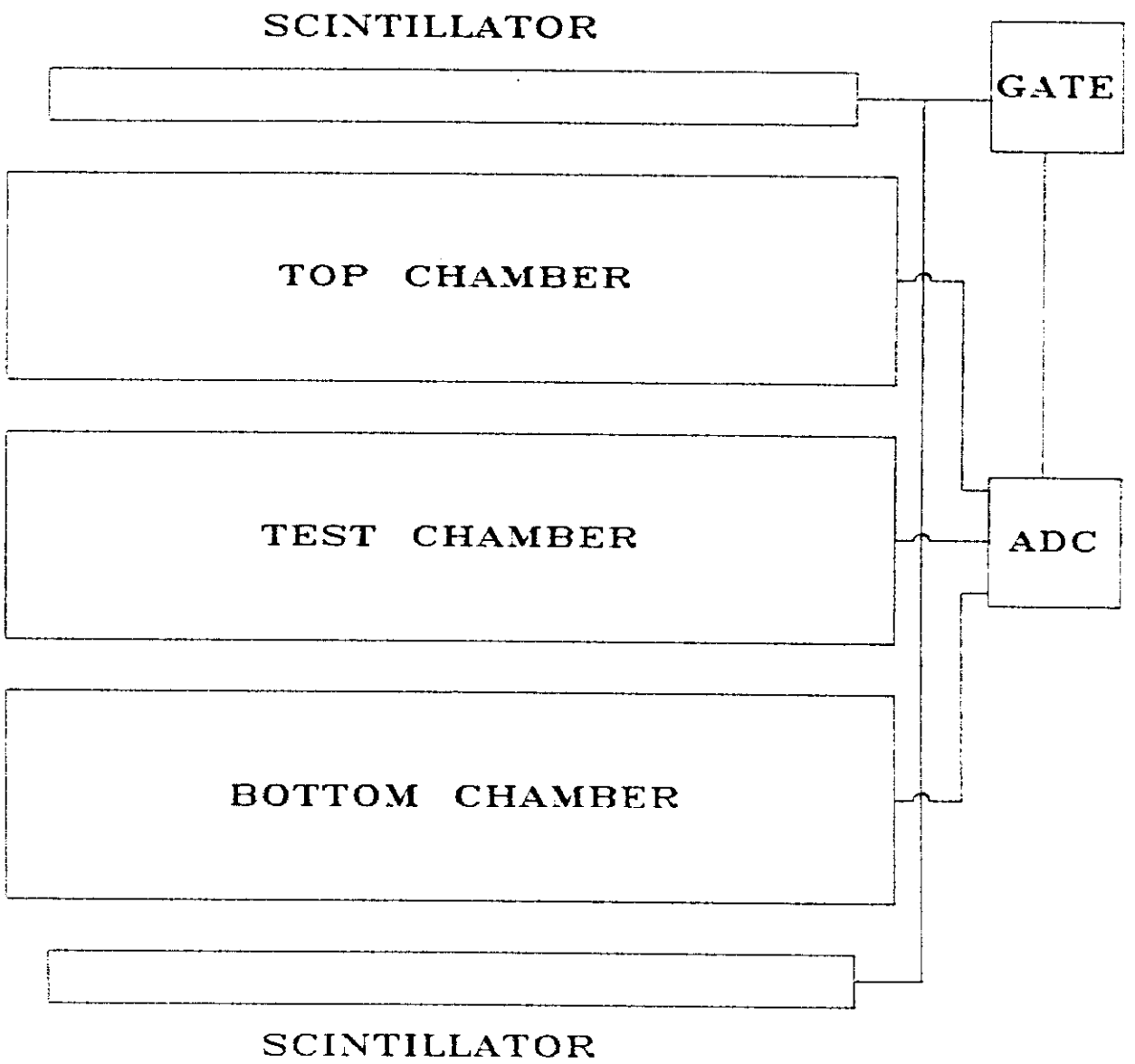
SCINTILLATOR
GATE
TOP CHAMBER
TEST CHAMBER
ADC
BOTTOM CHAMBER
SCINTILLATOR

Fig. 9

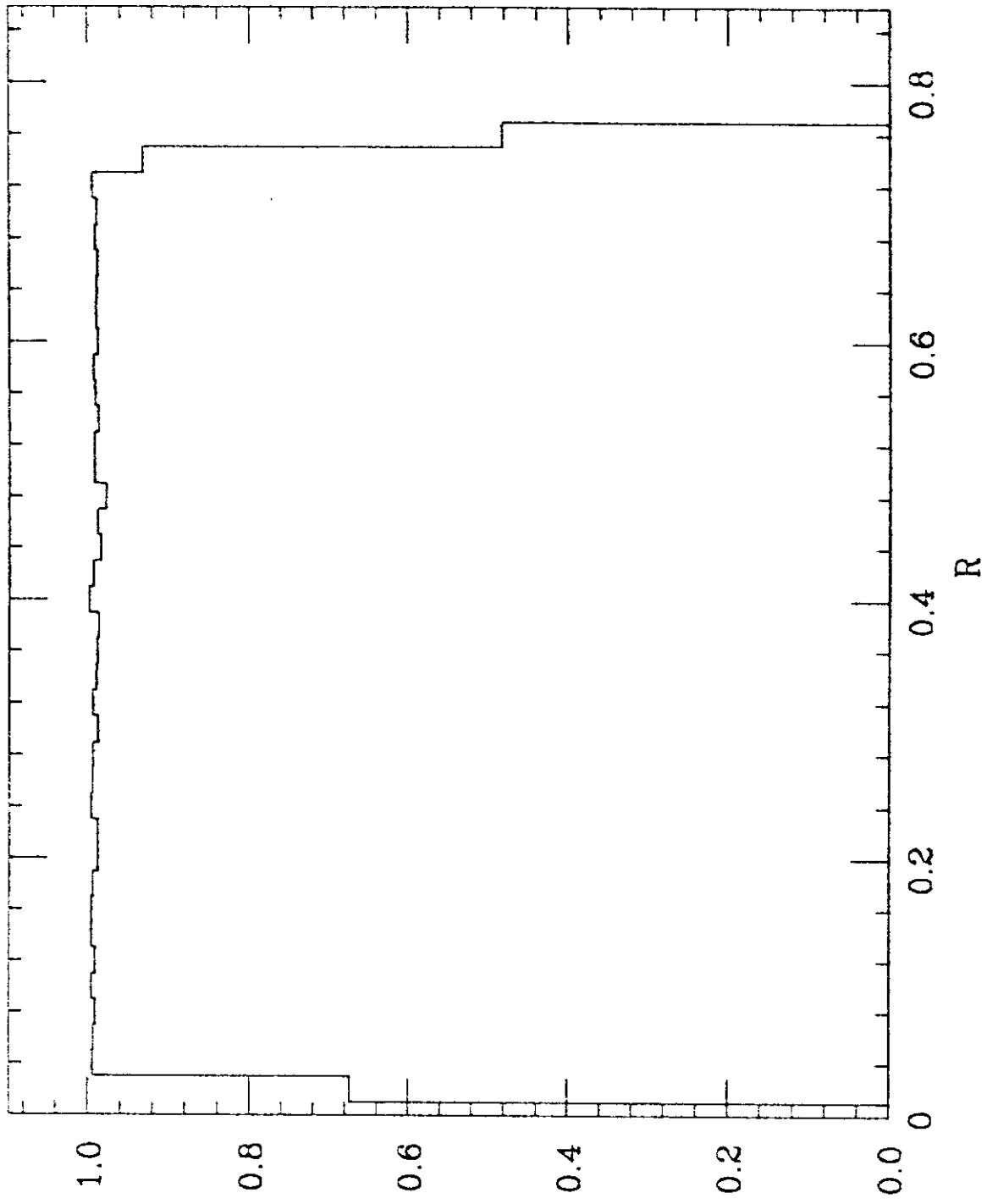

Fig. 10

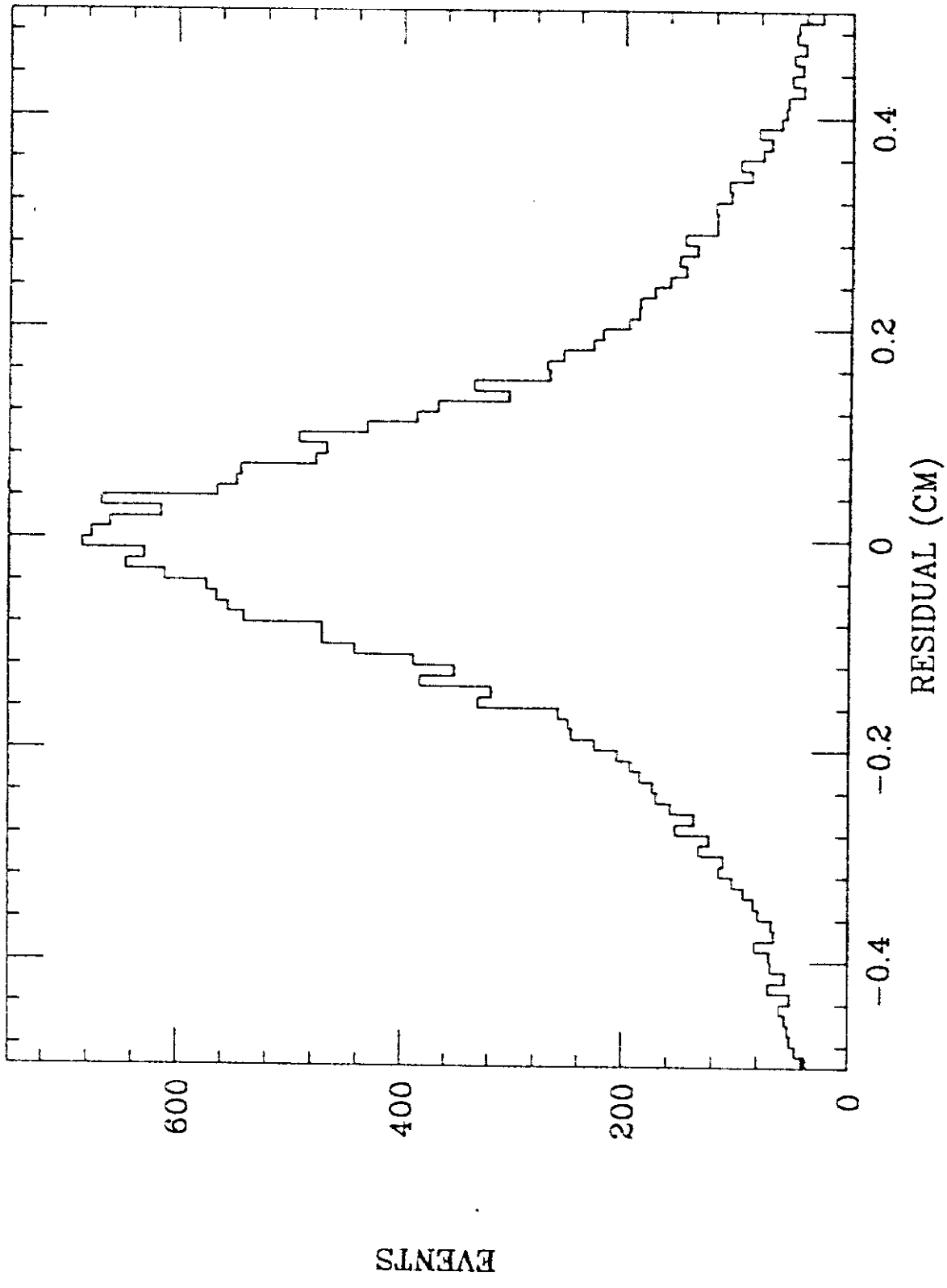

Fig. 11

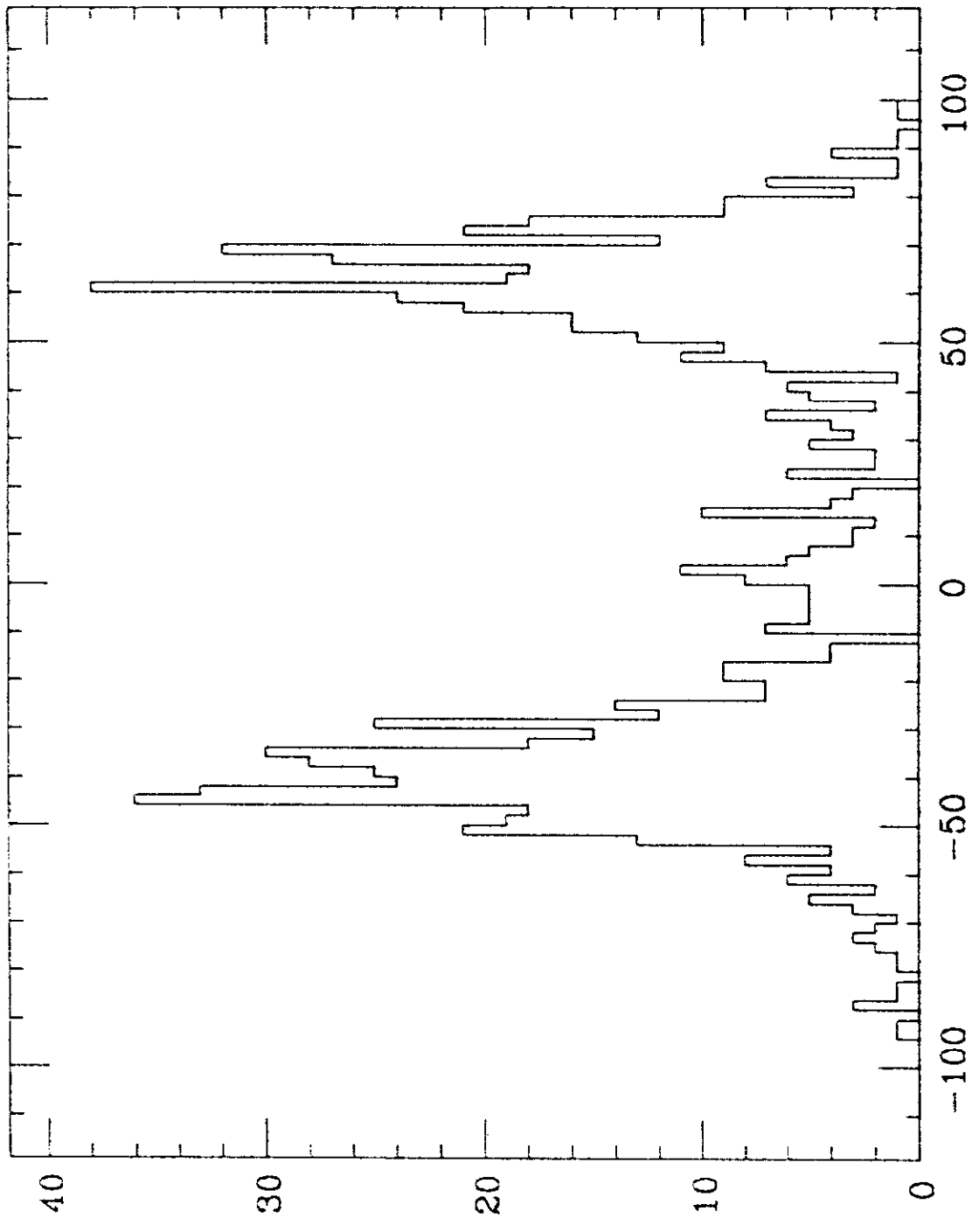

Fig. 12

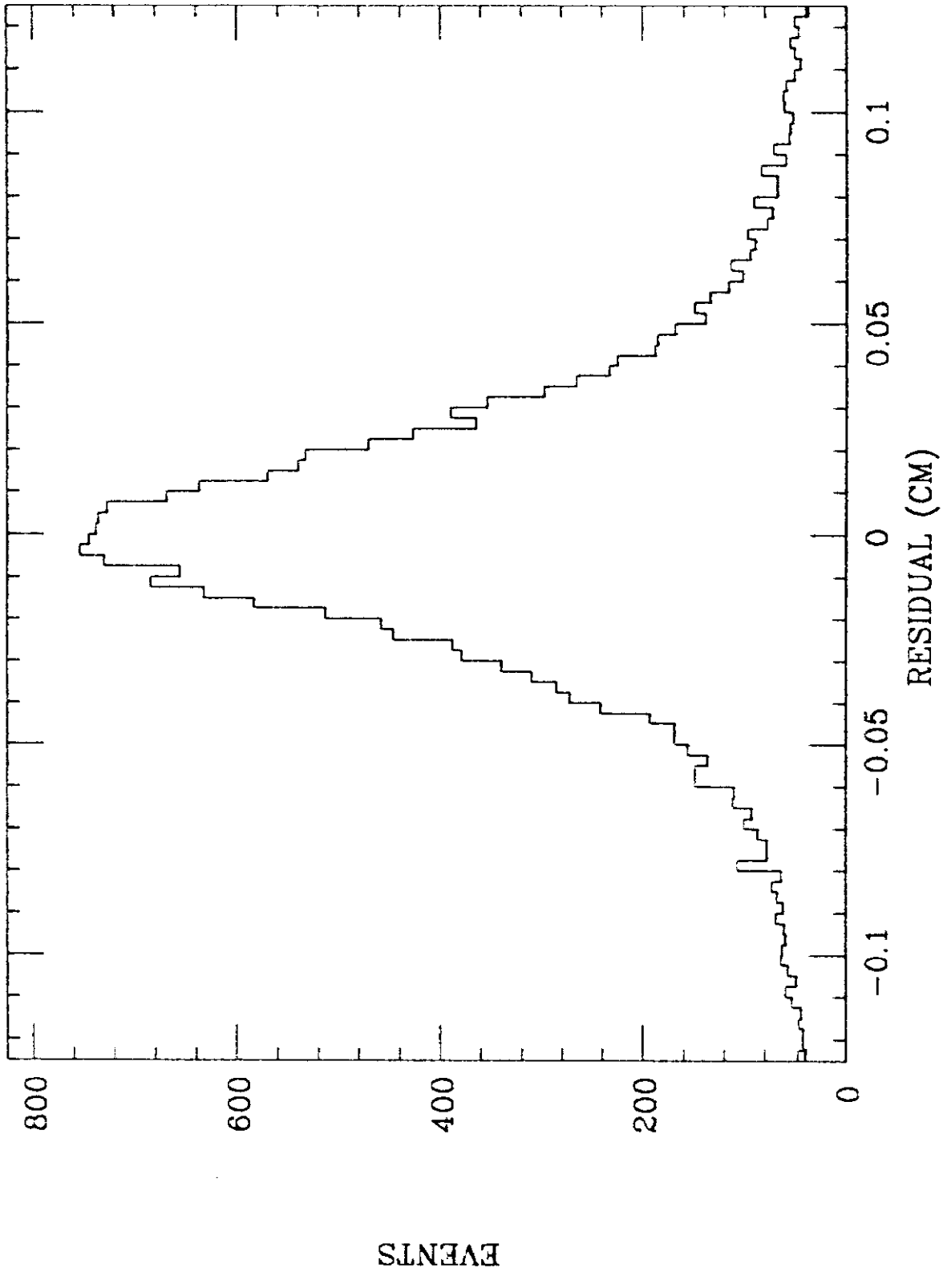

Fig. 13

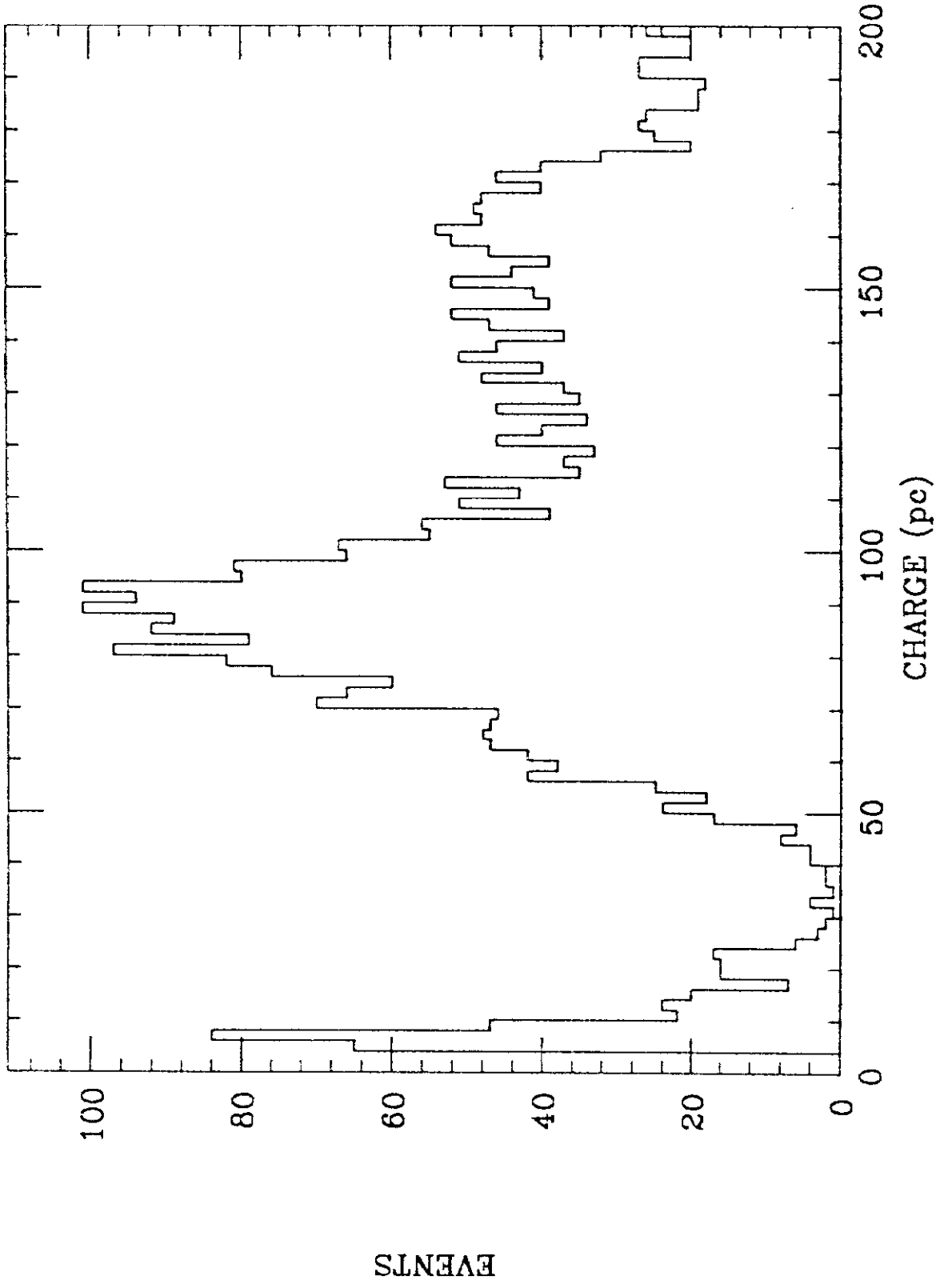

Fig. 14

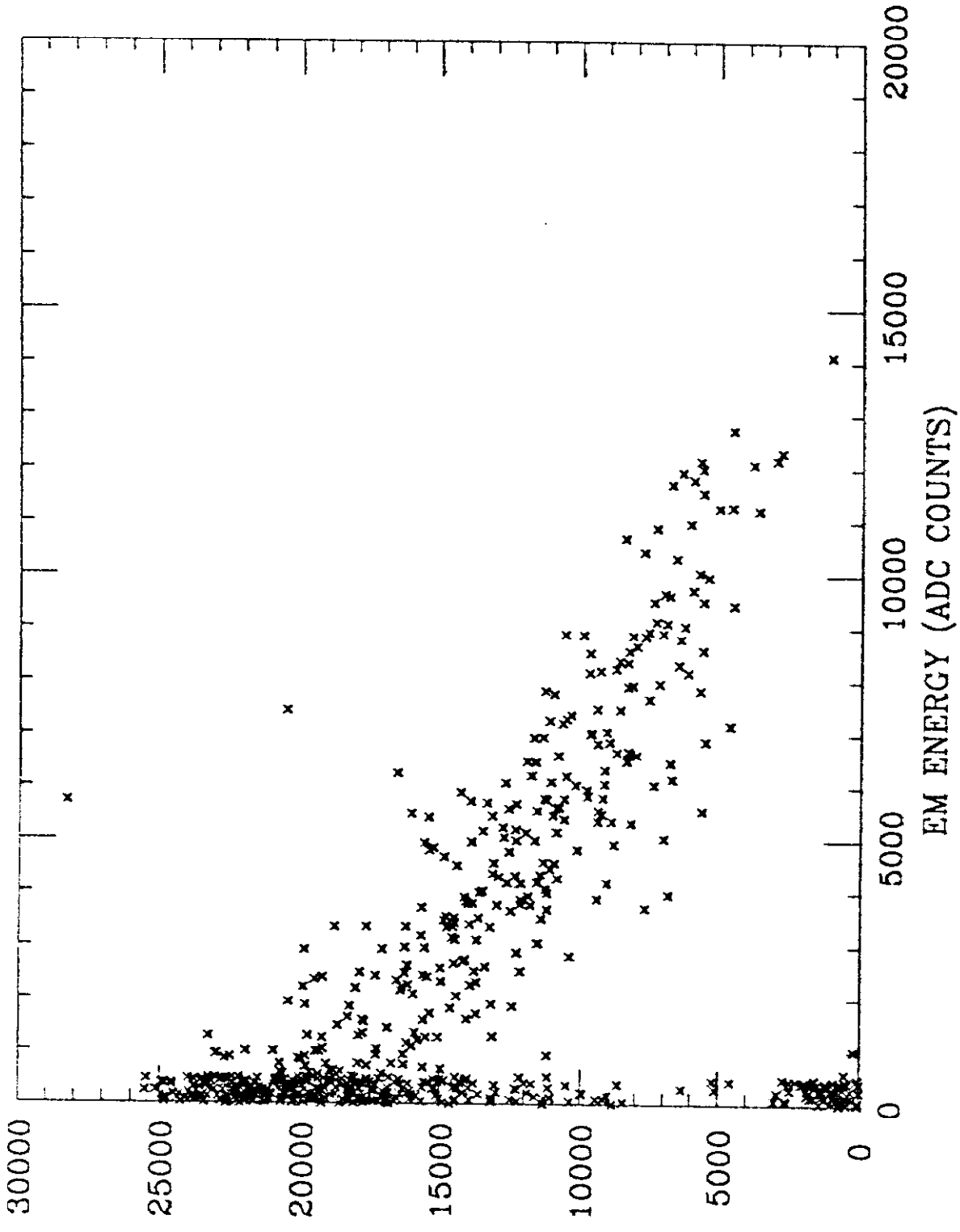
HADRON ENERGY (ADC COUNTS)
30000
25000
20000
15000
10000
5000
0
0
5000
10000
15000
20000
EM ENERGY (ADC COUNTS)

Fig. 15

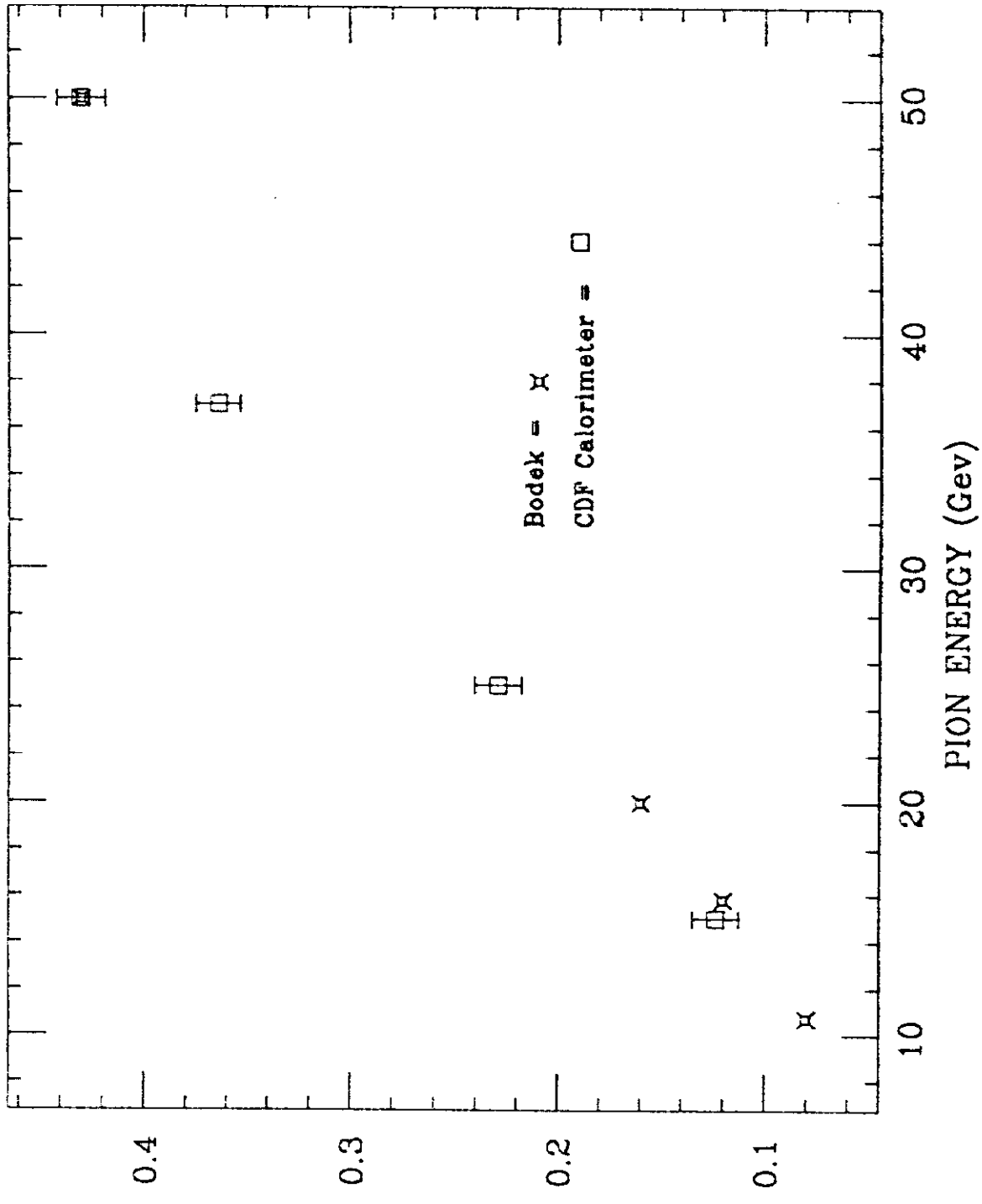
PUNCH THROUGH PROBABILITY
0.4
0.3
0.2
0.1
10
20
30
40
50
PION ENERGY (Gev)
Bodek =
CDF Calorimeter =

Fig. 16

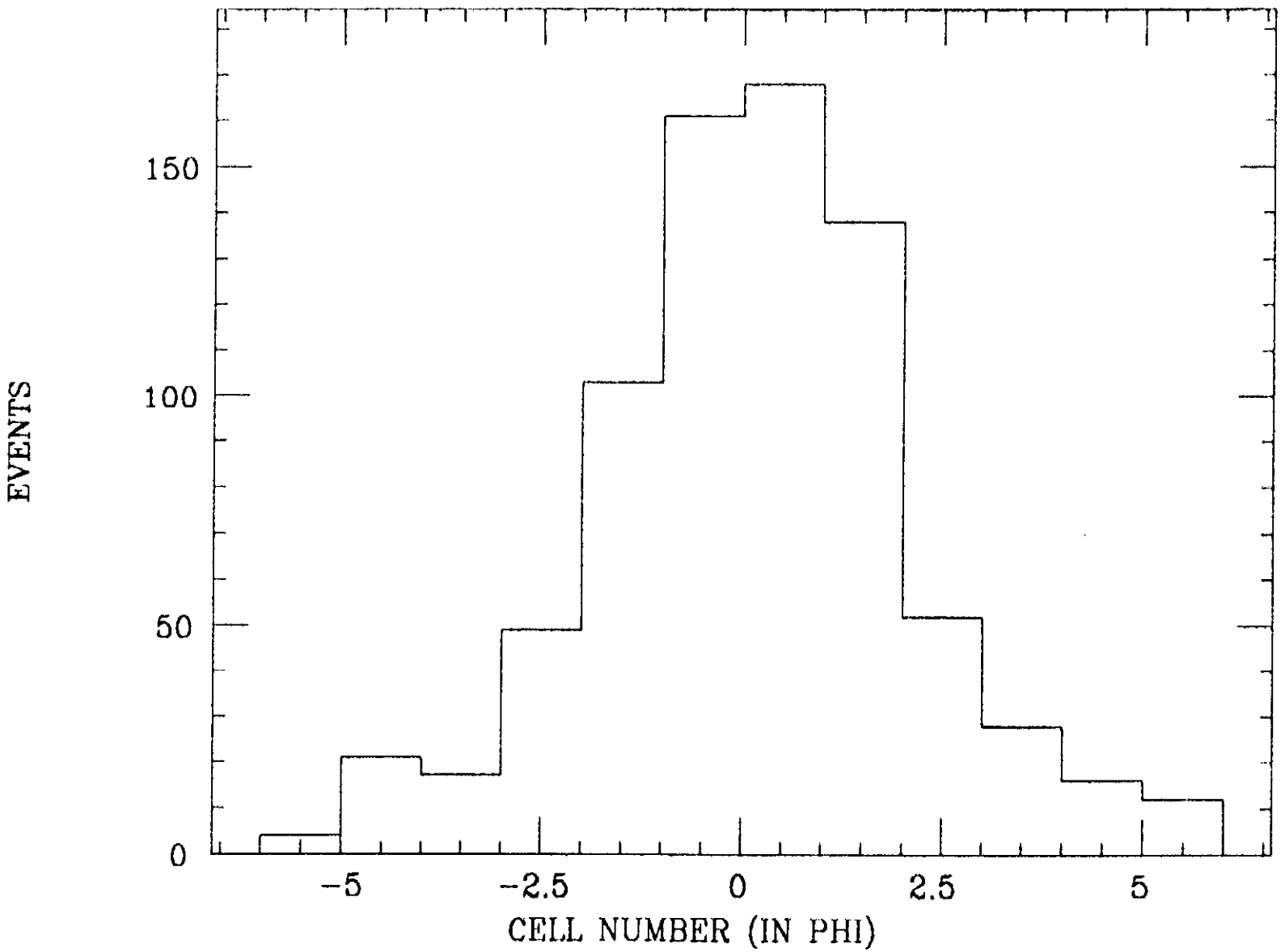

Fig. 17

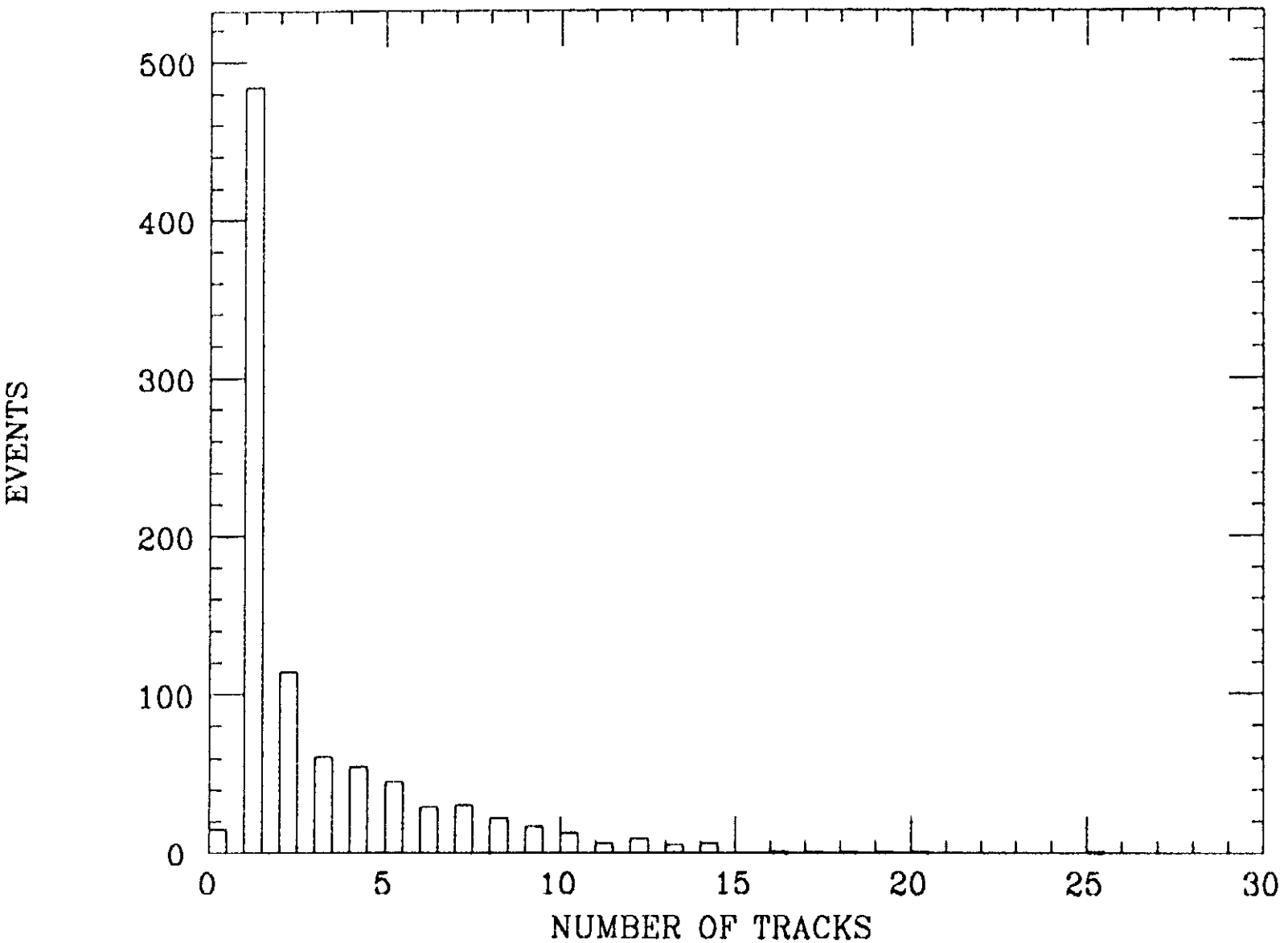

Fig. 18